Applied Mechanics and Materials *Online: 2019-06-10*
ISSN: 1662-7482, Vol. 892, pp 1-7
doi:10.4028/www.scientific.net/AMM.892.1

A Computational Study on Structural and Electronic Properties of 1-(4-Chlorophenyl)-2-{[5-(4-Chlorophenyl)-1,2,3-Oxadiazol-2-yl]sulfanyl}Ethanone

Pek-Lan Toh[1,a*], Montha Meepripruk[2,b] and Rosfayanti Rasmidi[3,c]

[1]Department of Electronic Engineering, Faculty of Engineering and Green Technology, Universiti Tunku Abdul Rahman, 31900, Perak, Malaysia

[2]School of Chemistry, Institute of Science and Technology, Kampheang Phet Rajabhat University, Kampheang Phet 62000, Thailand

[3]Faculty of Applied Sciences, Universiti Teknologi Mara Sabah, Locked Bag 71, 88997 Kota Kinabalu, Malaysia

[a]peklan_toh@yahoo.com.my, [b]montha_mee@hotmail.com, [c]rosfa270@sabah.uitm.edu.my

Keywords: Density Functional Theory, 1-(4-Chlorophenyl)-2-{[5-(4-chlorophenyl)-1,3,4-oxadiazol-2-yl]sulfanyl}ethanone, Geometrical Parameters, Electronic Structures.

Abstract. In this paper, a first principle Density Functional Theory (DFT) method was conducted to study the geometric and electronic structures of 1-(4-chlorophenyl)-2-{[5-(4-chlorophenyl) -1,3,4-oxadiazol-2-yl]sulfanyl}ethanone, $C_{16}H_{10}C_{l2}N_2O_2S$. Using B3LYP level of theory with four basis sets of 6-31G**, 6-31++G**, 6-311G**, and 6-311++G**, the equilibrium structure of the title molecule was used to determine the total energies, Frontier molecular orbital's energies, Mulliken atomic charges, and others. The computed findings present that four total energies obtained are close to each other, with the corresponding values of -59716.06 eV, -59709.42 eV, -59708.56 eV, and -59716.51 eV, respectively for B3LYP/6-31G**, B3LYP/6-31++G**, B3LYP/6-311G**, and B3LYP/6-311++G** methods. The calculated HOMO-LUMO energy gaps were predicted in the range of 4.001 eV - 4.089 eV. In this study, the atomic charge values of molecular system were also determined using Mulliken Population Analysis (MPA) approach. For DFT/B3LYP/6-311G** level of calculation, the computed results show that the atom of C_8 accommodates the highest negative charge in the title molecular system. All the oxygen, nitrogen, and chloride atoms are having negative charges, whereas all the hydrogen atoms are having positive charges. In addition, the dipole moment value was also determined to be 1.4758 Debye by employing DFT/B3LYP/6-311G** level of theory.

Introduction

Oxadiazole derivative are the heterocyclic compounds that have a very wide range of biological activities, namely antifungal, antiviral, antibacterial, antimicrobial, and others. Nowadays, the derivatives of oxadiazole have attracted wide attention in medicinal chemistry field [1-7]. For example, Husain and Ajmal (2009) synthesized and characterized a series of 1,3,4-oxadiazole derivatives using Fourier transform infrared (FT-IR), nuclear magnetic resonance (NMR), and mass spectrometry (MS) [1]. In addition, a lot of biological tests have also been conducted on these new synthesized oxadiazole derivatives. The results revealed that these derivatives of oxadiazole hold great potential as target for discovering new, safe and effective anti-inflammatory drug. In 2011, Kumar presented a new series of 2-amino-5-substituted-1,3,4-oxadiazole derivatives [2]. From this study, Kumar has successfully developed an environmentally benign synthetic method, which produces the derivatives of 2-amino-5-substituted-1,3,4-oxadiazole in excellent yields. Malhotra *et al.* (2012) synthesized and characterized new oxadiazole derivatives using using Raman spectroscopy, FT-IR spectroscopy, NMR spectroscopy, and mass spectrometry [3]. All synthesized oxadiazole derivatives were tested for some biological activities. The results show that there are only four synthesized compounds to `show the highest antifungal screening data. Also, the observation findings presented that these four compounds having additional substituents (nitro, methoxy, chloro,

bromo) at the *ortho* and *meta* positions, respectively. Bala and his co-workers, in 2014 synthesized and analyzed 1,3,4-Oxadiazole derivatives using UV, IR, NMR and mass spectrometry [4]. The molecular docking results found that one of synthesized compounds showed the most potent peptide deformylase inhibitor with the corresponding value of -153.44. In 2016, Vani *et al.* also synthesized and characterized triazole and oxadiazole derivatives using IR, NMR and mass spectrometry techniques [5]. Also, these title compounds were screened for their antibacterial and antifungal activities. In the same year, 1,3,4-Oxadiazole derivatives were synthesized and presented by Luo and his co-researchers [6]. These new compounds were also mainly evaluated for their activity against focal adhesion kinase. Kumar *et al.* (2017) also reported the crystal structure of 1-(4-chlorophenyl)-2-{[5-(4-chlorophenyl)-1,3,4-oxadiazol-2-yl]sulfanyl}ethanone, $C_{16}H_{10}Cl_2N_2O_2S$ [7]. Besides above experimental studies, there is also a lot of relevant computational and theoretical research works on the oxadiazole derivatives. For example, in 2013, Soleiman-Beigi and his co-workers studied the solvent effect on structures and properties of 1,3,4-oxadiazole-2-thiol derivatives using B3LYP/6-311++G** level of theory [8]. The calculated solvent effect values are quite consistent with those of experimental results. Wang *et al.* (2014) studied the molecular structure of 5,5'-bis(naphthalen-2-yl)-2,2'-bi(1,3,4-oxadiazole) using B3LYP, CAM-B3LYP, and M062x functionals with 6-311+G** basis set [9]. The computed findings showed that the vibrational frequencies of title compound obtained with B3LYP/6-311+G** method are quite close to the values obtained from the experiment. Unfortunately, there was almost no written literature on $C_{16}H_{10}Cl_2N_2O_2S$.In order to further exploit the existing knowledge for finding new, safe, and effective drugs, the fundamental studies of $C_{16}H_{10}Cl_2N_2O_2S$ have played extremely important roles. In this paper, the geometrical parameters and electronic structures of $C_{16}H_{10}Cl_2N_2O_2S$ were determined using first principle Density Functional Theory (DFT) method. The details of computational methodology, results, discussion, and summary will be discussed in the following sections.

Computational Methodology

In this study, all Density Functional Theory (DFT) calculations of $C_{16}H_{10}Cl_2N_2O_2S$ wrere carried out with Gaussian 09 and GaussView 5 software packages [10]. A single-molecule of $C_{16}H_{10}Cl_2N_2O_2S$ was chosen as the local molecular environment in the calculation. Fig. 1 illustrates the molecular structure of the title compound. Using geometry optimization calculations, the local energy minima of $C_{16}H_{10}Cl_2N_2O_2S$ were obtained at B3LYP level of theory, with employing four different basis sets (6-31G**, 6-31++G**, 6-311G**, and 6-311++G**). The optimized geometries were then used to determine the total energy values using single point calculations. In addition, the other electronic properties such as energy difference between the highest occupied molecular orbital (HOMO) and lowest unoccupied molecular orbital (LUMO), atomic charge, and others are also predicted in this work.

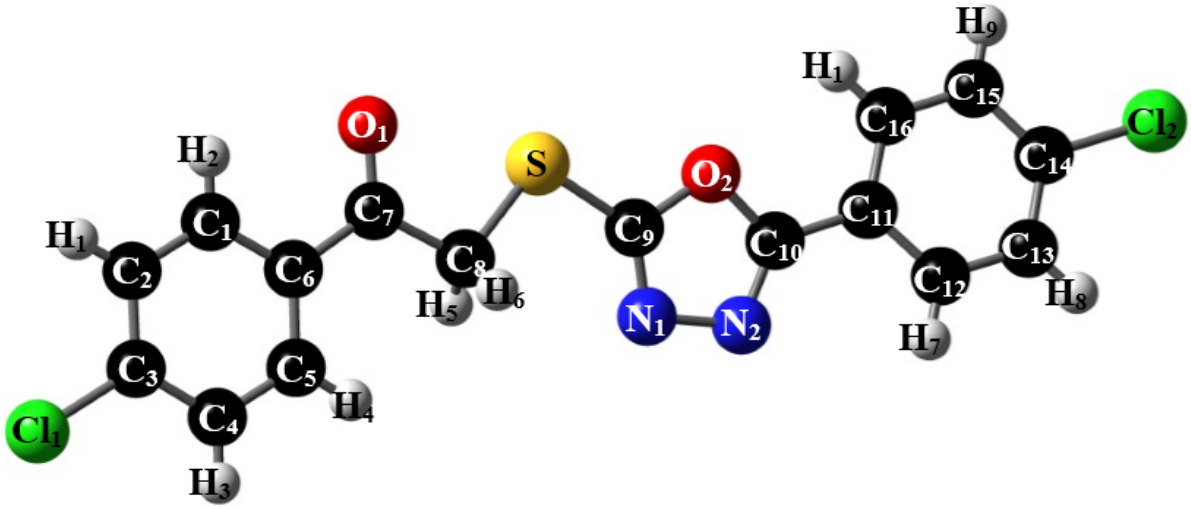

Fig. 1. Molecular structure of $C_{16}H_{10}Cl_2N_2O_2S$ with the numbering of atoms.

Results and Discussion

Table 1 presents the geometrical parameters (bond distances, bond angles, and dihedral angles) of $C_{16}H_{10}Cl_2N_2O_2S$ using B3LYP level of theory with employing four basis sets (6-31G**, 6-31++G**, 6-311G**, and 6-311++G**). As can be seen from the table, the overall calculated bond distances obtained with density functional theory method are close to those of experimental values [7]. This is because of the computational results belong to isolated molecule in the gaseous phase, whereas the experimental findings belong to molecules in solid state phase. For example, the Cl_1-C_3 bonds are having the bond lengths in the range of 1.752 Å to 1.753 Å. These computed bond distance values are about 1.0% larger than the measurement value (1.735 Å). The C_8-S bond lengths for the DFT method with employing all four basis sets (B3LYP/6-31G**, B3LYP/6-31++G**, B3LYP/6-311G**, and B3LYP/6-311++G**) are calculated in the range of 1.833 Å - 1.836 Å. These simulated values are about 1.9% longer than the experimental C_8-S bond length.

Table 1. Experimental and calculated geometrical parameters using DFT/B3LYP level of theory with employing four basis sets of $C_{16}H_{10}Cl_2N_2O_2S$.

	B3LYP/ 6-31G**	B3LYP/ 6-31++G**	B3LYP/ 6-311G**	B3LYP/ 6-311++G**	Exp [7]
Bond distance (Å)					
Cl_1-C_3	1.752	1.752	1.753	1.752	1.735
C_7-O_1	1.221	1.222	1.214	1.215	1.219
C_8-S	1.834	1.836	1.833	1.834	1.801
C_9-S	1.748	1.748	1.747	1.746	1.728
N_1-N_2	1.397	1.396	1.396	1.396	1.424
C_{10}-C_{11}	1.457	1.458	1.456	1.456	1.460
C_{14}-Cl_2	1.755	1.755	1.756	1.755	1.740
Bond angle (°)					
C_6-C_7-C_8	117.6	117.6	117.4	117.4	119.9
C_8-S-C_9	97.4	97.5	97.4	97.5	100.0
C_9-O_2-C_{10}	102.1	102.3	102.1	102.3	102.0
Dihedral angle (°)					
C_7-C_8-S-C_9	183.6	183.7	183.6	183.7	183.7
C_8-S-C_9-O_2	192.0	192.1	192.1	192.1	190.8

While the bond lengths calculated for N_1-N_2 are about 2.0% shorter than the experimental value (1.424 Å). The corresponding N_1-N_2bond distance values are between 1.396 Å and 1.397 Å at the DFT/B3LYP level of calculation with four basis sets of 6-31G**, 6-31++G**, 6-311G**, and 6-311++G**. Also can be seen in Table 1, the bond and dihedral angles obtained with DFT calculations are very good agreement with experiment [7]. The results note that DFT/B3LYP calculations are one of powerful approaches for understanding the geometrical parameters of title molecular system. The simulated C_6-C_7-C_8 and C_8-S-C_9 bond angles are about 2.7% smaller than the experimental values, whereas the bond angles of C_9-O_2-C_{10} obtained with DFT simulations are about 0.3% larger than the measurement bond angle (102.0°). In the case of dihedral angles, the computed angles are only 0.6% larger and smaller than the experimental data.

The calculated total energy values are summarized in Table 2. According to the data from the table, the four total energies obtained are quite close to each other using DFT/B3LYP level of theory with employing four basis sets. The corresponding energy values are -59716.06 eV, -59709.42 eV, -59708.56 eV, and -59716.51 eV, respectively for 6-31G**, 6-31++G**, 6-311G**, and 6-311++G** basis sets. Moreover, the results of Frontier molecular orbital's energies are presented in Table 2. These Frontier molecular orbital's energies are very important in this study because of it helps to characterize the chemical reactivity and kinetic stability of the title compound. In addition, it also helps to obtain the optical and electrical properties of the title molecular system. In order to determine the above energetic behaviors of the title molecule, the energy values of HOMO and LUMO are determined. For HOMO, the four corresponding energy values obtained are -6.524 eV, -6.537 eV, -6.297 eV, and -6.584 for DFT/B3LYP/6-31G**, DFT/B3LYP/6-31++G**, DFT/B3LYP/6-311G**, and DFT/B3LYP/6-311++G** level of calculations, respectively. While, the energies of LUMOs are -2.434 eV, -2.536 eV, -2.215 eV, and -2.551, respectively for the DFT method with employing all four basis sets (B3LYP/6-31G**, B3LYP/6-31++G**, B3LYP/6-311G**, and B3LYP/6-311++G**). The results noted that the computed LUMOs are mostly anti-bonding type orbitals. In this study, the energy gap of HOMO-LUMO is the energy separation between HOMO and LUMO. The four calculated HOMO-LUMO energy gaps obtained from DFT calculations are close to each other, which fall in the range of 4.001 eV - 4.089 eV. Fig. 2 shows the illustration of frontier molecular orbitals obtained from B3LYP/6-311G** level of calculation, with their corresponding positive and negative regions. The molecular orbital analysis shows that HOMO is delocalized on the parts of furan and chlorobenzene, and the lone pair of electron on the sulfur atom, whereas LUMO shows the anti-bonding character with π-distributed on the another group of chlorobenzene in the molecular system. In the figure, we also found that HOMO-1 and HOMO-2 have almost equal charge densities, which are delocalized on whole of the molecular system. Similarly, LUMO has a higher charge density than LUMO+2.

Table 2. Total and HOMO-LUMO energies (eV) of $C_{16}H_{10}Cl_2N_2O_2S$.

	B3LYP/ 6-31G**	B3LYP/ 6-31++G**	B3LYP/ 6-311G**	B3LYP/ 6-311++G**
Total energy	-59716.066	-59709.416	-59708.560	-59716.506
HOMO	-6.524	-6.537	-6.297	-6.584
LUMO	-2.434	-2.536	-2.215	-2.551
HOMO-LUMO gap	4.089	4.001	4.082	4.033

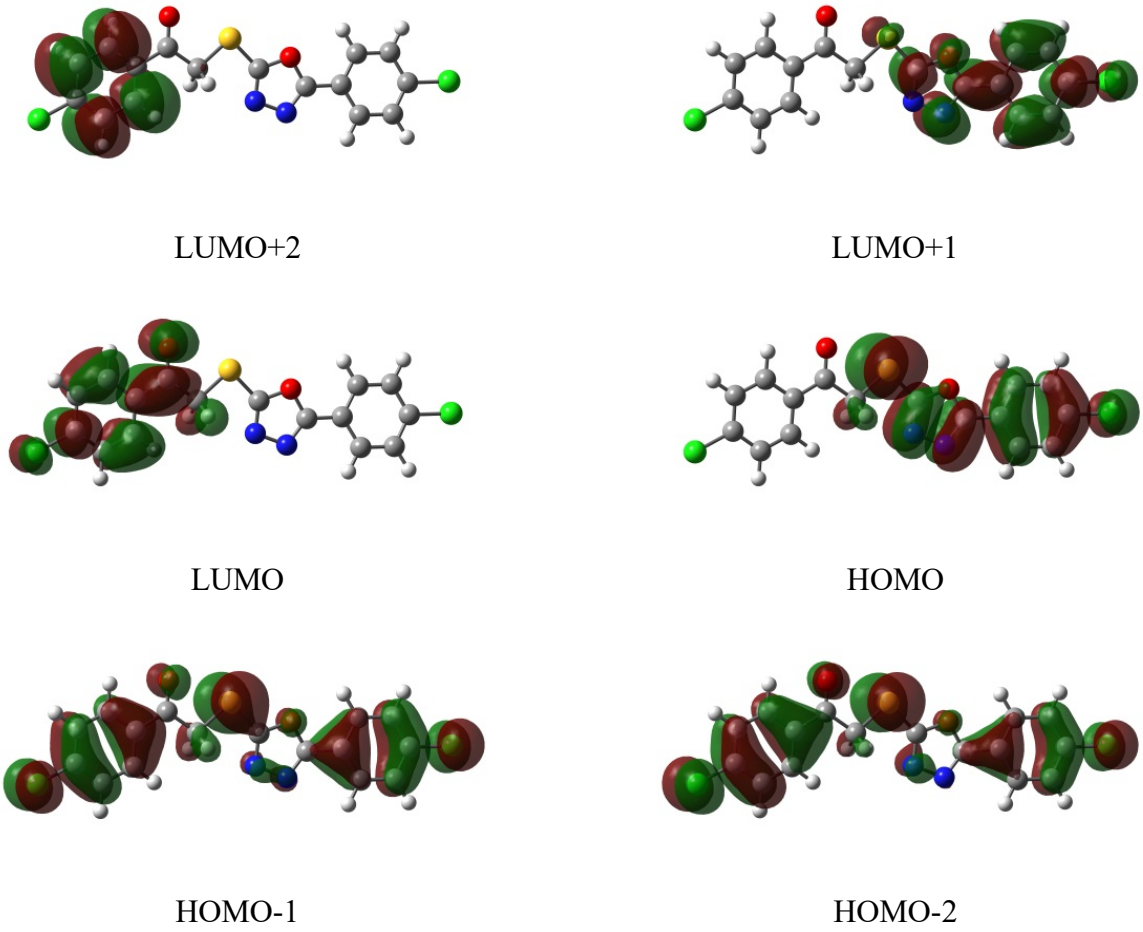

Fig. 2. Frontier molecular orbitals (MOs) of $C_{16}H_{10}Cl_2N_2O_2S$ with DFT/B3LYP/6-311G** in the gaseous phase.

Molecular electrostatic potential (MEP) surfaces for $C_{16}H_{10}Cl_2N_2O_2S$ model computed using DFT method with B3LYP/6-311G** level of theory as shown in Fig. 3. As can be seen from the figure, we noted that the distribution of molecular electrostatic potential surface depends on the negative and positive charge distribution. The atoms of O_1 and N_1 have maximum electron densities because of the region around these two atoms show the red color surfaces, whereas the rest of molecule is surrounded by yellow and green colors, which shows the difference in electronegativity is not great. Based on the results, we also noted that the intermolecular and intramolecular hydrogen bonding may possible to occur at these sites. The Mulliken atomic charges of the tile compound at the B3LYP/6-31G** level of theory are illustrated in Fig. 4. This Mulliken atomic charge calculation plays an important role in predicting the properties of the quantum chemical calculations of the molecular system. It is because the atomic charges will then be affected the dipole moment in the molecular system. Based on Mulliken Population Analysis (MPA) scheme, the atom of C_8 has the highest negative charge value (-0.406) in the calculation. The result indicates that this site is the most favorable sites of protonation and methylation in the molecular system. According to the data from the figure, the negative charges are also found on oxygen, nitrogen, and chlorine atoms. The atoms of C_1, C_3, C_5, C_6, C_{11}, C_{12}, C_{14}, and C_{16} in the tile compound have negative charges. On the contrary, the other carbon atoms in the molecular system have positive charges. Moreover, the charges of hydrogen atoms are all positive, which fall in the range of 0.113 - 0.195. In this paper, the dipole moment of the tile molecular system at DFT/B3LYP/6-311G** method is 1.4758 Debye.

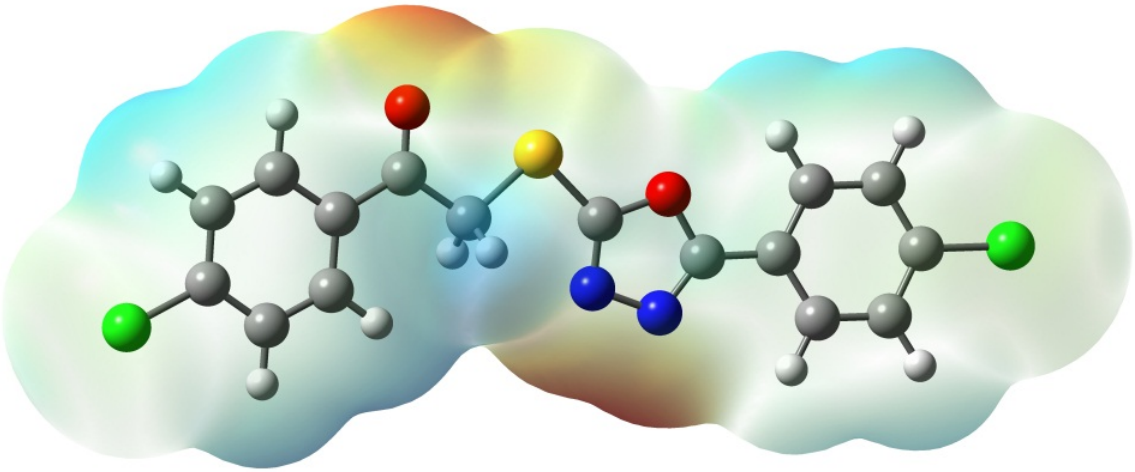

Fig. 3. Molecular electrostatic potential surface of $C_{16}H_{10}Cl_2N_2O_2S$ using DFT/B3LYP/6-311G** level of theory.

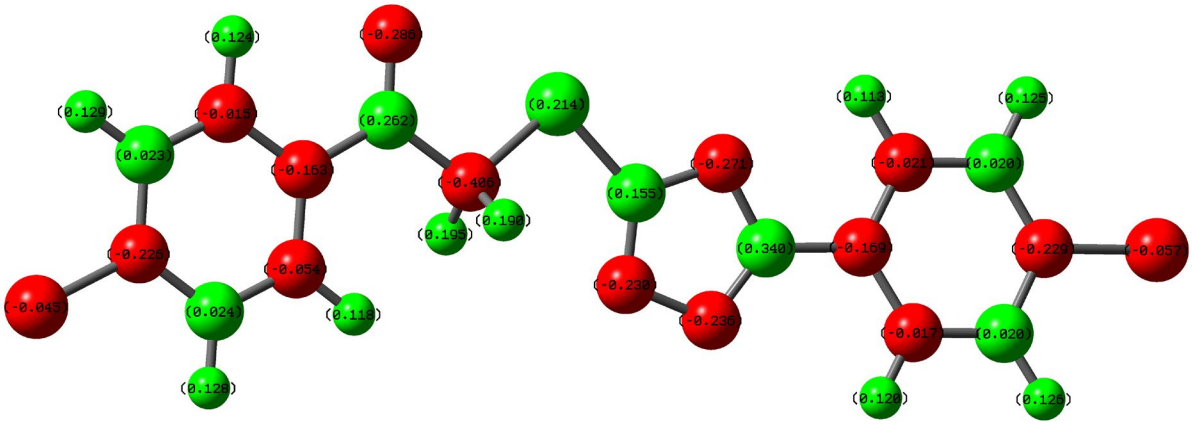

Fig. 4. Mulliken atomic charge distribution of $C_{16}H_{10}Cl_2N_2O_2S$ using DFT/B3LYP/6-311G** level of calculation.

Conclusion

In this study, all DFT calculations were conducted using Gaussian 09 and GaussView 5 software programs. Using B3LYP level of theory with employing four different basis sets of 6-31G**, 6-31++G**, 6-311G**, and 6-311++G**, the geometrical parameters and electronic properties of the tile compound were determined. The equilibrium geometries of the tile compound were found using geometry optimization calculation. The equilibrium structure of the molecular system was then used to determine the total energy, Mulliken atomic charges, and others. The computed results found that the optimized geometry shows a good agreement with the similar experimental results [7]. Four total energies obtained are quite close to each other using B3LYP level of theory with employing four different basis sets (6-31G**, 6-31++G**, 6-311G**, and 6-311++G**). Moreover, four HOMO-LUMO energy values obtained are close to each other, which fall in the range of 4.001 eV - 4.089 eV. Based on the scheme of MPA, C_8 atom calculated by DFT/B3LYP/6-311G** level of

calculation has the highest negative charge, and this site is most favorable sites of protonation and methylation in the tile compound. Also, the calculated dipole moment obtained is 1.4758 Debye in the DFT/B3LYP/6-311G** method.

References

[1] A. Husain, M. Ajmal, Synthesis of novel 1,3,4-oxadiazole derivatives and their biological properties, Acta Pharm. 59 (2009) 223-233.

[2] S. Kumar, Synthesis of some 2-amino-5-substituted-1,3,4-oxadiazole derivatives in the acetic acid, E-J. Chem. 8 (2011) S448-S454.

[3] M. Malhotra, M. Sanduja, A. Samad and A. Deep, A. New oxadiazole derivatives of isonicotinohydrazide in the search for antimicrobial agents: Synthesis and in vitro evaluation, J. Serb. Chem. Soc. 77(1) (2012) 9-16.

[4] S. Bala, S. Kamboj, V. Saini, and D. N. Prasad, 1,3,4-Oxadiazole Derivatives: Synthesis, Characterization, Antimicrobial Potential, and Computational Studies, BioMed Research International 2014 (2014) 172791-1-18.

[5] K. V. Vani, G. Ramesh, C. V. Rao, Synthesis of new triazole and oxadiazole derivatives of quinazolin-4(3H)-one and their antimicrobial activity, J. Heterocyclic Chem. 53 (2016) 719-726.

[6] Y. Luo, Z. J. Liu, G. Chen, J. Shi, J. R. Li, H. L. Zhu, 1,3,4-. Oxadiazole derivatives as potential antitumor agents: Discovery, optimization and biological activity valuation. MedChemComm 7(2) (2016) 263-271.

[7] R. Kumar, S. Hussain, K. M. Khan, S. Perveen, S. Yousuf, Crystal structure and Hirshfeld surface analysis of 1-(4-chloro-phen-yl)-2-{[5-(4-chloro-phen-yl)-1,3,4-oxa-diazol-2-yl]sulfan-yl}ethanone, ActaCryst. E. 73 (2017) 524-527.

[8] M. Soleiman-Beigi, R. Aryan, M. Yousofizadeh, and Sh. Khosravi, A combined synthetic and DFT study on the catalyst-free and solvent-assisted synthesis of 1,3,4-oxadiazole-2-thiol derivatives, J. Chem. (2013) 476358-1-6.

[9] H. Wang, F. Q. Bai, X. Jia, D. Cao, R. M. Kumar, J. L. Brédas, S. Qu, B. Bai, H. X. Zhang and M. Li, Theoretical study on molecular packing and electronic structure of bi-1,3,4-oxadiazole derivatives, RSC Adv. 4 (2014) 51942-51949.

[10] M. J. Frisch, G. W. Trucks, H. B. Schlegel, G. E. Scuseria, M. A. Robb, J. R. Cheeseman, G. Scalmani, V. Barone, G. A. Petersson, H. Nakatsuji, X. Li, M. Caricato, A. V. Marenich, J. Bloino, B. G. Janesko, R. Gomperts, B. Mennucci, H. P. Hratchian, J. V. Ortiz, A. F. Izmaylov, J. L. Sonnenberg, D. Williams-Young, F. Ding, F. Lipparini, F. Egidi, J. Goings, B. Peng, A. Petrone, T. Henderson, D. Ranasinghe, V. G. Zakrzewski, J. Gao, N. Rega, G. Zheng, W. Liang, M. Hada, M. Ehara, K. Toyota, R. Fukuda, J. Hasegawa, M. Ishida, T. Nakajima, Y. Honda, O. Kitao, H. Nakai, T. Vreven, K. Throssell, J. A. Montgomery, Jr., J. E. Peralta, F. Ogliaro, M. J. Bearpark, J. J. Heyd, E. N. Brothers, K. N. Kudin, V. N. Staroverov, T. A. Keith, R. Kobayashi, J. Normand, K. Raghavachari, A. P. Rendell, J. C. Burant, S. S. Iyengar, J. Tomasi, M. Cossi, J. M. Millam, M. Klene, C. Adamo, R. Cammi, J. W. Ochterski, R. L. Martin, K. Morokuma, O. Farkas, J. B. Foresman, and D. J. Fox, Gaussian 09, Revision E.01, Gaussian, Inc., Wallingford CT, 2016.